Thermal Resistance of Open-cell Metal Foam with Thermal Pad

Fathiah Zaib*, P. Ganesan, Tuan Zaharinie

Department of Mechanical Engineering, Faculty of Engineering, Universiti of Malaya, 50603, Kuala Lumpur, Malaysia

*Corresponding Author
doi: https://doi.org/10.21467/proceedings.141.26

ABSTRACT

This paper investigates the thermal resistance of sandwich structures consisting of open-type metal foams, base plate/surface and Thermal Interface Material (TIM) (thermal pad type). Two types of sandwiched study samples: Types 1 and 2, were investigated. The samples were prepared using metal foam structures, i.e., 20, 40, 60 PPI, and two commercial thermal pads, i.e., PC93, and PC94. The samples' thermal resistance and thickness were measured under the compression loadings of 0 - 60 N using a thermal resistance tester that was developed in-house according to ASTM D5470 standard. The nanoindentation test indicated that PC93 had slightly higher hardness than PC94, with 0.0007 and 0.0004 GPa, reflecting their softness. The result shows that the samples' thermal resistance is affected by compression force and decreases as compression load increases. The thermal resistance of the PC94 sample was reduced to 58% at 30 N load for 60 PPI, Type 1 configuration. The resistance decreases by 5% when the PPI increases from 20 to 60 PPI. This study demonstrates that joining metal foam, thermal pad, and base plate could reduce thermal resistance while increasing performance. It also provides insights into an alternative means of joining metal foams with other metals (or a base plate) in the development of heat exchangers.

Keywords: Open-cell metal foam, thermal interface material (TIM), thermal pad, thermal resistance.

1 Introduction

Open-type metal foam is a porous medium with a solid metal matrix with empty or fluid-filled voids [1]. A metal foam's number of pores per inch (PPI) ranges from 5 to 100, with probably a very high porosity (ε), i.e., up to 0.98 or 0.99 [2]. Open-cell metal foams have high thermal conductivity, and a large surface area [3]. Therefore, metal foams are suitable for heat sink applications, such as an open-cell aluminium foam heat sink (40 PPI; $\varepsilon = 0.9$) for electronic cooling [4]. It can also be useful in various heat exchanger applications like metal foam heat exchangers (30 PPI; $0.8 < \varepsilon < 0.9$) for automotive exhaust gas recirculation (EGR) systems [5]. Studies have also used thermal interface materials (TIM) as a thermal coupling between mating parts. TIM eliminates air traps between the conjoined surfaces and decreases contact resistance and thermal impedance [6]. Several types of TIMs are commercially available in different forms, such as thermal grease [7], solder [8], phase change material (PCM) [9, 10], thermal adhesive epoxy [11], and thermal film or pad [12-14].

A TIM heat transfer performance can be affected by several factors, including compression loading, thickness, thermal conductivity, and hardness. Sim et al. (2005) found that compression on a test sample can decrease the thermal resistance due to the reduction of the air gap on the sandwich surfaces [16]. Meanwhile, Kanetsuki et al. (2016) found that thermal resistance for joints under 20 MPa bonding was lower than that in 3 MPa bonding (0.038 and 0.039 mm^2K/W, respectively). They concluded that controlling bonding pressure is critical to reduce numbers of voids in the bonded section. Studies have found that high thermal conductivity improves the thermal resistance for heat flow through a TIM sample [18]. Thus, a good TIM material should demonstrate high intrinsic thermal conductivity. Yu et al. (2012)

Proceedings DOI: 10.21467/proceedings.141; Series: AIJR Proceedings; ISSN: 2582-3922; ISBN: 978-81-957605-4-1

tested TIMs using silver paste and silver nanoparticles. The study reported a low thermal resistance ranging from 5 to 30 mm²K/W and from 0.2 to 5.5 mm²K/W, respectively. In this regard, a soft pad TIM is advantageous as a softer TIM is easily deformed by slight contact pressure to ensure good interface conformity [20]. In this light, a soft pad TIM is easier to handle and can be compressed up to 25% of its total thickness.

This study aims to measure the total thermal resistance decrement of sandwiched samples with open-type copper (Cu) metal foam, Cu base plates and TIMs of pad types. A TIM tester, developed in-house following ASTM D5470, is used for measurements. The sandwiched study samples are built for two different configurations, namely Types 1 and 2, using metal foam structures of 20, 40, and 60 PPI and several commercial TIMs based on pad types (i.e., PC93 and PC94).

2 Materials and Methods

2.1 Preparation of samples (TIM, metal foam, and copper plate)

Two different types of thermal pads were tested in this study were purchased from reliable manufacturers, T-Global Technology Co., Ltd. Thermal pads PC93 and PC94 are made from the same materials, polyolefin copolymer (15%) and aluminium oxide (85%), and according to the supplier data, PC93 and PC94 have the same hardness of 60 shores 00. However, they have different thicknesses and thermal conductivity of 1 and 2 mm, and 2 and 4 W/mK, respectively [21, 22].

For the sample preparations, the thermal pad was cut into 18 mm x 18 mm. Cu metal foams of 20, 40, and 60 PPI and 5 mm thick were purchased from Linyi Gelon LIB Co., Ltd. (Shandong, China). The Cu foams were cut into 18 mm x 18 mm using Sodic A500W Wire Electrical Discharge Machining (EDM). Cu plates of 1 mm thickness of 18 mm x 18 mm were used as a base plate/surface to sandwich the thermal pad and the metal foams.

Two types of samples were prepared using the combination of plate, thermal pad, and metal foams (Figure 1a). For Type 1, a metal foam was sandwiched between two pads and plates to investigate the heat transfer through the pad and foam. For Type 2, a set of two metal foams and a thermal pad was sandwiched between two thermal pads and plates (Figure 1b) to investigate the heat transfer from foam to another foam through TIM. 12 samples were prepared from different combinations of setups, metal foams PPI, and thermal pad types. Another six samples were prepared without any TIM for Type 1 (NoTIM-T1) and Type 2 (NoTIM-T2) for comparison purposes.

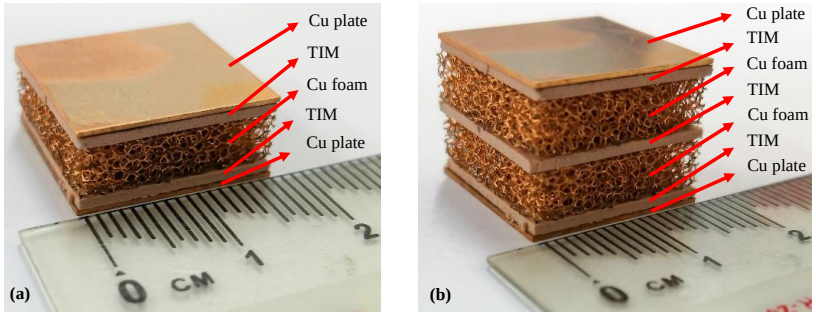

Figure 1: *(a) Type 1 configuration and (b) Type 2 configuration.*

For measurement, inspections, and quality checks, micrographs of the metal foam's structure were obtained using a scanning electron microscope (SEM; Thermo Scientific^{FM} Phenom Prox). The image of ligaments and pores was taken for all metal foams. The compositional analysis of the foam samples and plates was determined using SEM energy dispersive X-ray spectroscopy (EDS). ImageJ software Version 1.51k was

Proceedings DOI: 10.21467/proceedings.141
ISBN: 978-81-957605-4-1

Series: AIJR Proceedings
ISSN: 2582-3922

used to analyse SEM images and measure the ligaments and pore size of the metal foams. Nanoindentation test was conducted to characterise the hardness and Young's modulus of TIM using a Hysitron TI 750Ubi™ scanning nanoindentation system with a Performech™ control unit and continuous stiffness measurement technique (CSM).

2.2 Thermal resistance tester

For this study, a thermal resistance tester was developed according to the ASTM D5470 standard to measure the thermal resistance of the samples at different compression loadings of 0 to 60 N. An electrical heater was located at the top (i.e., aluminium heating bar 50 x 50 x 60 mm) while the heat sink was at the bottom (i.e., aluminium cooling bar). The bar of k: 167 W/mK was attached with a 150 w cartridge heater to achieve a constant temperature of 80 ºC. The heat sink below the aluminium cooling bar (50 x 50 x 90 mm) of the tester was based on the continuous running of tap water at a temperature inlet, $T_{w,\,in}$ and temperature outlet, $T_{w,\,out}$, around 24 and 27 ℃, respectively. Two dial gauges with a maximum range of 12.7 mm and a resolution of 0.001 mm were used to measure sample loading during the test. Six thermal resistance detector (RTD) temperature sensors (Maltec, Japan; Accuracy Class A), Ø3.2 x 30 length and accuracy: ± 0.05 ºC were installed on the top and bottom aluminium bars. Eight compression springs at bottom of the tester (oil tempered wire with k: 0.0312 kg/mm) were used to calculate the pressure measured using the length value of the spring being pressed. The schematic in Figure 2b shows the locations of the temperature sensors for T_1 to T_6 in the bars. An RTD Temperature Data Logger (OctRTD) was used to record the temperature data. Meanwhile, a temperature controller connects with the cartridge heater to supply a specific heat temperature to the aluminium bar.

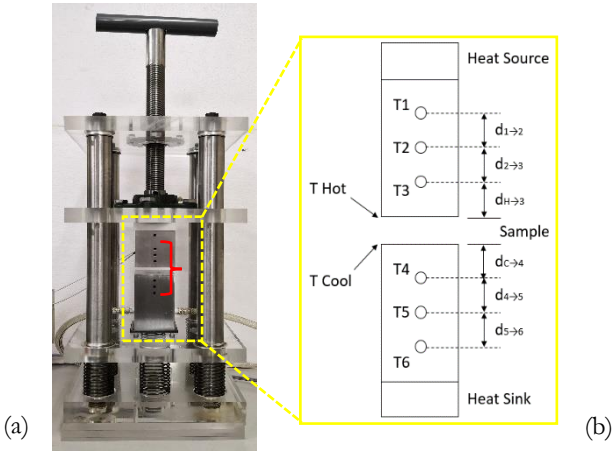

Figure 2: *(a) Experimental facility developed for thermal resistance tester, (b) Schematic of RTD locations from T_1 to T_6 at the aluminium bar.*

The heat flux, Q, labelled as Q_{hot} at the top aluminium bar and Q_{cold} at the bottom of the aluminium bar, were calculated based on the temperature differences at the aluminium bar. The total heat flux through the sample was calculated as an average of Q_{hot} and Q_{cold}. The formulation details are given as follows,

$$Q_{hot} = k_m A\left[\frac{\Delta T_{1\to3}}{d_{1\to3}}\right] \quad ; \quad Q_{cold} = k_m A\left[\frac{\Delta T_{1\to3}}{d_{1\to3}}\right] \quad ; \quad Q = \frac{(Q_{hot} + Q_{cold})}{2} \qquad (1)$$

Where K_m is the thermal conductivity of aluminium bar, A is the area of meter bar mating surfaces, ΔT is the temperature difference at points 1 to 3, and d is the distance between two points, e.g., $d_{1\to3}$ is the distance from point 1 to 3. It is impossible to directly measure the aluminium bar's hot surface temperature (Ths)

and cold surface temperature (Tcs). Therefore, T_{hs} and T_{cs} were calculated based on the temperature drop in the top and bottom aluminium bar as shown below,

$$T_{hs} = T_3\left[\frac{d_{3\to h}}{d_{1\to 3}}\right]T_1 - T_3 \quad ; \quad T_{cs} = T_4\left[\frac{d_{c\to 4}}{d_{4\to 6}}\right]T_4 - T_6 \tag{2}$$

Then, thermal resistance, R_{th} (℃/W), could be determined by,

$$R_{th} = \frac{T_{hs} - T_{cs}}{Q} \tag{3}$$

An uncertainty analysis was performed to quantify the uncertainty in each measured quantity, resulting in the overall uncertainty in the thermal resistance of the samples under test. The uncertainty in each quantity in Eqs. 1–3 was obtained using the Taylor method [23]. Thus, the maximum uncertainty for the measurement was calculated as follows,

$$\frac{\partial R}{R} = \left(\left(\frac{\partial Q}{Q}\right)^2 + \left(\frac{\partial \Delta T}{T}\right)^2 + \left(\frac{\partial d}{d}\right)^2 + \left(\frac{\partial t}{t}\right)^2 + \left(\frac{\partial A}{A}\right)^2 + \left(\frac{\partial F}{F}\right)^2\right)^{1/2} \tag{4}$$

The main uncertainty in the experiment was the errors in determining the heat flux through the sample, 3.3%. The maximum uncertainties for the RTD sensors and the data acquisition readings were ±0.05 ℃ with a maximum error of 1.8% between the mating surfaces of the sample and the aluminium bar. The uncertainties of compression samples thickness (0.8%), area (2.1%), and compression loading (2.7%) were included in the uncertainty's measurement. In this study, the maximum uncertainty was estimated to be ±5.2%.

2.3 Experimental procedure

Before any testing, the surfaces of the aluminium bar interface that would come into contact with the study samples were cleaned using acetone. Each sample was then placed on the surface of the bottom bar (cool side), and the top heater bar was moved to be in contact with the sample. At this condition, the compression force to the sample is near zero. The aluminium bars are insulated to reduce heat loss. Then, continuous running of the tap water through a heat sink was released constantly to cold down the bottom bar for heat transfer circulation. A temperature controller from the thermal resistance tester was set to 80 ℃ when the samples and insulations were set up. The test was started once the temperature was stable (no fluctuation temperature) and data collection was carried out beyond the first 10 minutes. During the compression process, temperature data were recorded every 2 N compressions, with data being collected every 10 seconds for one minute. The increment load was a relatively small incremental force. The compression force (N) gradually increased manually by 0 to 60 N. There was no significant fluctuation of the temperature data implying a good steady condition along the test. There were three duplicates for each sample type for repeatability measurements, and only average data was presented in the later section.

3 Results and discussion

3.1 Microstructural observation and analysis

The images of ligaments and pores of metal foams were taken using SEM. Examples are given in Figures 3a and b, which show pores and ligament of 60 PPI foam at 400X and 620X magnification, respectively. A cross-section view at 500X magnification, as in Figure 3c, reveals that the ligament is hollow and seen for all metal foams.

Proceedings DOI: 10.21467/proceedings.141
ISBN: 978-81-957605-4-1

Series: AIJR Proceedings
ISSN: 2582-3922

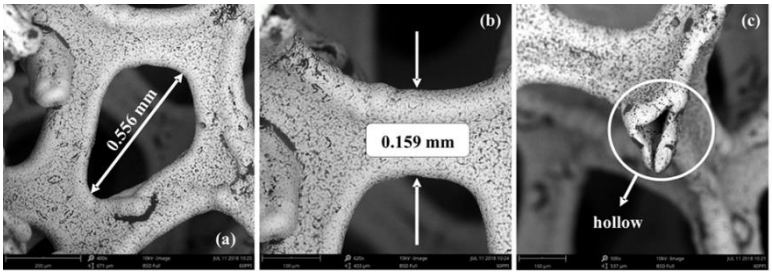

Figure 3: *Samples of SEM images of 60 PPI foam of (a) pore size at 410X magnifications, (b) ligament size at 620X magnification, and (c) hollow ligament of porous structure at 500X magnification.*

The compositional analysis of the foam samples using EDS confirmed that the compositions of Cu material in the 20, 40, and 60 PPI foam samples were 100%. EDS tests were done and indicated that the Cu foam and plates were examined with 100% Cu composition.

3.2 Nanoindentation test

Figure 4a shows the loads (μN) as a function of penetration depth (nm) from a nanoindentation test for different TIMs. The penetration depth was significantly deep for PC93 and PC94, reflecting their soft characteristic. PC94 has the most shift curve compared to PC93 in this case. Figure 4b shows the hardness of the tested pads. It was found that PC94 pad has a slightly higher hardness value compared to PC93 which were 0.004 GPa and 0.007 GPa, respectively, reflecting their softness characteristic.

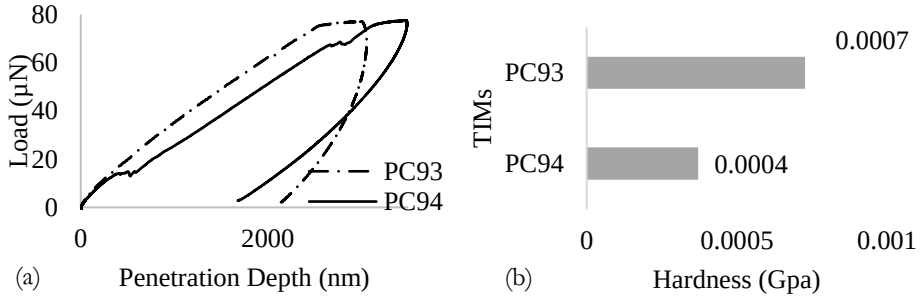

Figure 4: *(a) Load displacement curve of TIMs, (b) Hardness of thermal pads*

3.3 The thermal resistance of thermal pads

The thermal resistance of PC93 and PC94 samples at different compression loads (N) is shown in Figure 5 based on 20, 40, and 60 PPI metal foams of Types 1 and 2 configurations. In general, the thermal resistance decreases with the increase of the compression force. It drops steeply from 0 to 10 N and then decreases gradually until 60 N.

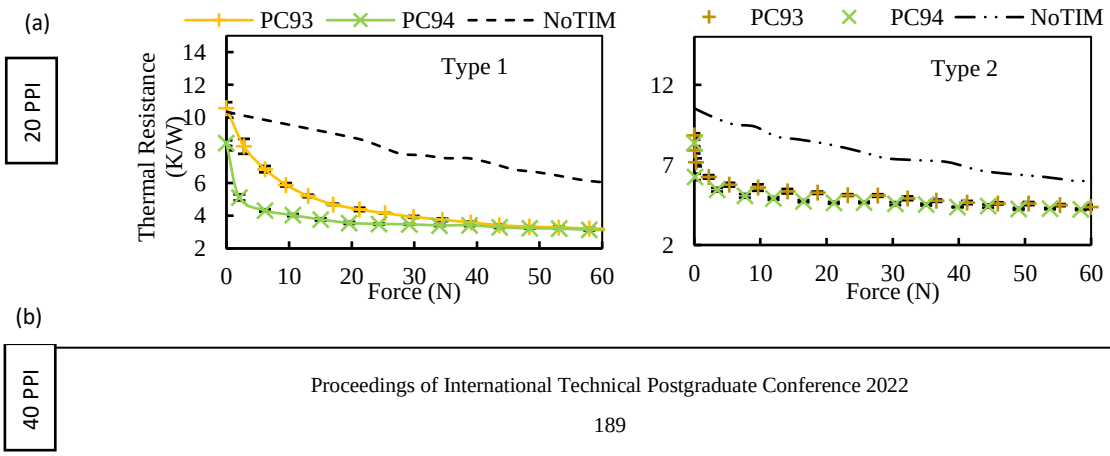

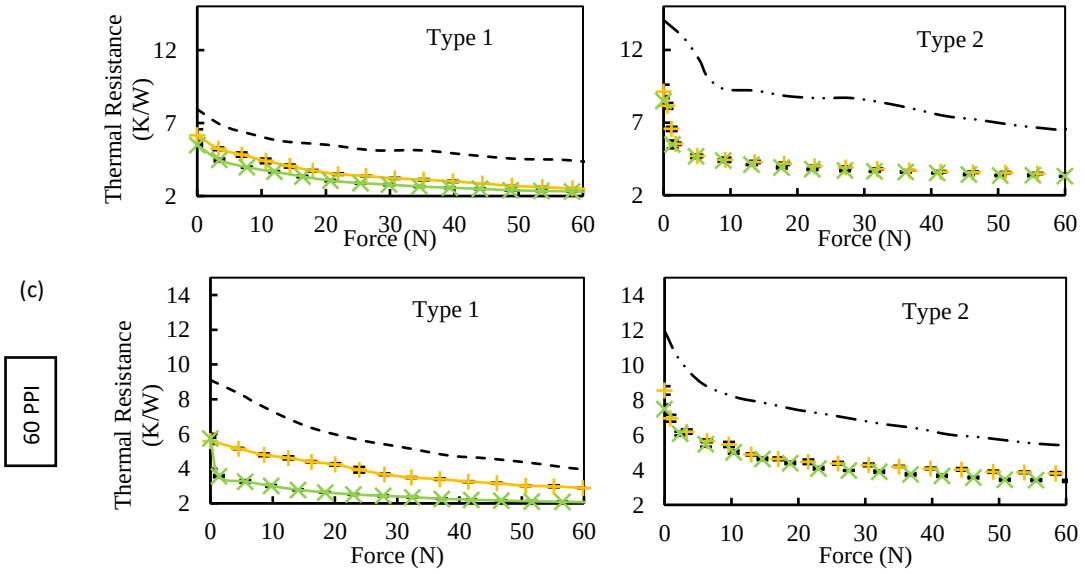

Figure 5: *Thermal resistance of thermal pad samples of (a) 20 PPI, (b) 40 PPI, and (c) 60 PPI for Type 1 and Type 2.*

The thermal resistance of PC94 was lower than PC93. Concerning the Type 1 setup, the result was understandable as PC94 was slightly softer, thinner (1 mm), and had a higher thermal conductivity value (4 W/mK) compared to PC93, which had 2 mm thick and k: 2 W/mK. PC94 had resulted in perfect contact with the metal foams where the ligaments of the metal foams pierce into the pads and fill the foam pores after the compression loading and thus, eliminating the air gap and increasing the thermal contact area between mating surfaces. Meanwhile, some of the PC93 pads had deformed to the side of the samples as the TIM was quite thick and cannot fill into the small foam pores and affecting the thermal resistance consequently. The difference in the thermal resistance between PC93 and PC94 was obvious. The thermal resistance of the TIM samples was significantly lower than the NoTIM samples. For example, the difference was 51%, 48%, and 50% for 20, 40 and 60 PPI, respectively, for 50 N by comparing NoTIM and PC94. When comparing Type 2 with Type 1, in general, the thermal resistance of Type 2 was higher than Type 1. This result could be expected due to the difference in the sample thickness, whereby Type 2 samples were two times thicker.

4 Conclusions

The resistance of the sandwiched samples using open-type metal foams and commercial TIMs was measured experimentally. The following are the conclusions from this study.

- PC94 had lower thermal resistance than PC93. The thermal resistance of the PC94 sample decreased to 58% at 30 N load for 60 PPI, Type 1. The thermal contact enhancement (compared with NoTIM samples) of PC94 increase a maximum of 55% under the same condition.
- Low hardness / softer TIM allows the ligament of foam to be filled with TIM during compression load; it increased the contact area between the ligaments and the surface when the foam was embedded within the soft TIM. Thus, it helped in reducing the thermal resistance and demonstrates a better heat transfer flow through the samples.

Proceedings DOI: 10.21467/proceedings.141
ISBN: 978-81-957605-4-1

Series: AIJR Proceedings
ISSN: 2582-3922

5 Declarations

5.1 Acknowledgements

This study was funded by the Universiti Malaya Impact-oriented Interdisciplinary Research Grant (IIRG005A-2020IISS) and the Ministry of Higher Education, Fundamental Research Grant Scheme (FRGS: FP052-2015A).

Nomenclature

A	Interface area (m^2)
k	Thermal conductivity (W/mK)
H	Hardness (GPa)
R_{th}	Thermal resistance
$T_{w, in}$	Temperature water inlet
$T_{w, out}$	Temperature water outlet

5.2 Competing Interests

There is no conflict of interest.

5.3 Publisher's Note

AIJR remains neutral with regard to jurisdiction claims in published maps and institutional affiliations.

References

[1] A. N. M. Alhusseny, A. Nasser, And N. M. Al-Zurfi, *High-Porosity Metal Foams: Potentials, Applications, And Formulations*. Intechopen, 2018.

[2] N. Dukhan, *Metal Foams: Fundamentals And Applications*. Destech Publications, Inc, 2013.

[3] T. Lu, H. Stone, And M. Ashby, "Heat Transfer In Open-Cell Metal Foams Acta Mater," 1998.

[4] A. Bayomy, M. Saghir, And T. Yousefi, "Electronic Cooling Using Water Flow In Aluminum Metal Foam Heat Sink: Experimental And Numerical Approach," *International Journal Of Thermal Sciences*, Vol. 109, Pp. 182-200, 2016.

[5] A. Muley, C. Kiser, B. Sundén, And R. K. Shah, "Foam Heat Exchangers: A Technology Assessment," *Heat Transfer Engineering*, Vol. 33, No. 1, Pp. 42-51, 2012.

[6] K. M. Shahil And A. A. Balandin, "Graphene–Multilayer Graphene Nanocomposites As Highly Efficient Thermal Interface Materials," *Nano Letters*, Vol. 12, No. 2, Pp. 861-867, 2012.

[7] S. Seki, R. Endoh, And M. Takeda, "Evaluation Of Thermal Resistance Of Various Thermal Grease," In *2018 International Conference On Electronics Packaging And Imaps All Asia Conference (Icep-Iaac)*, 2018: Ieee, Pp. 576-578.

[8] C. Deppisch *Et Al.*, "The Material Optimization And Reliability Characterization Of An Indium-Solder Thermal Interface Material For Cpu Packaging," *Jom*, Vol. 58, No. 6, Pp. 67-74, 2006.

[9] C. Jia, X. Geng, F. Liu, And Y. Gao, "Thermal Behavior Improvement Of Hollow Sintered Bricks Integrated With Both Thermal Insulation Material (Tim) And Phase-Change Material (Pcm)," *Case Studies In Thermal Engineering*, Vol. 25, P. 100938, 2021.

[10] S. D. Sharma, H. Kitano, And K. Sagara, "Phase Change Materials For Low Temperature Solar Thermal Applications," *Res. Rep. Fac. Eng. Mie Univ*, Vol. 29, No. 1, Pp. 31-64, 2004.

[11] J. Li *Et Al.*, "Enhanced Thermal Transport Properties Of Epoxy Resin Thermal Interface Materials," *Es Energy & Environment*, Vol. 4, No. 6, Pp. 41-47, 2019.

[12] S. Shanmugan, D. Mutharasu, And A. H. Haslan, "A Study On Aln Thin Film As Thermal Interface Material For High Power Led," *Int. J. Electron. Comput. Sci. Eng.*, Vol. 2, No. 1, Pp. 296-300, 2012.

[13] J. Xu, A. Munari, E. Dalton, A. Mathewson, And K. M. Razeeb, "Silver Nanowire Array-Polymer Composite As Thermal Interface Material," *Journal Of Applied Physics*, Vol. 106, No. 12, P. 124310, 2009.

[14] L. Zhao, S. Chu, X. Chen, And G. Chu, "Efficient Heat Conducting Liquid Metal/Cnt Pads With Thermal Interface Materials," *Bulletin Of Materials Science*, Vol. 42, No. 4, Pp. 1-5, 2019.

[15] L. C. Sim, S. Ramanan, H. Ismail, K. Seetharamu, And T. Goh, "Thermal Characterization Of Al2o3 And Zno Reinforced Silicone Rubber As Thermal Pads For Heat Dissipation Purposes," *Thermochimica Acta*, Vol. 430, No. 1-2, Pp. 155-165, 2005.

[16] Y. J. Lee, "Thermo-Mechanical Properties Of High Performance Thermal Interface Gap Filler Pads," In *2010 12th Ieee Intersociety Conference On Thermal And Thermomechanical Phenomena In Electronic Systems*, 2010: Ieee, Pp. 1-8.

[17] S. Kanetsuki, S. Miyake, K. Kuwahara, And T. Namazu, "Influence Of Bonding Pressure On Thermal Resistance In Reactively-Bonded Solder Joints," *Japanese Journal Of Applied Physics*, Vol. 55, No. 6s1, P. 06gp17, 2016.

[18] H. Yu, L. Li, And Y. Zhang, "Silver Nanoparticle-Based Thermal Interface Materials With Ultra-Low Thermal Resistance For Power Electronics Applications," *Scripta Materialia*, Vol. 66, No. 11, Pp. 931-934, 2012.

[19] H. Yu, R. Zhang, L. Li, X. Mao, And H. Du, "Silver-Based Thermal Interface Materials With Low Thermal Resistance," In *2012 13th International Conference On Electronic Packaging Technology & High Density Packaging*, 2012: Ieee, Pp. 410-413.

[20] J. Meth, S. Zane, M. Demko, T. Mai, R. Pryor, And H. Salerno, "Thermal And Mechanical Properties Of Vertically Aligned Carbon Fiber Epoxy Composites," In *2016 32nd Thermal Measurement, Modeling & Management Symposium (Semi-Therm)*, 2016: Ieee, Pp. 95-98.

[21] T. Global. "Pc93-150x150x1.0 -Thermal Pad, Non-Silicone, 150mm X 150mm X 1mm, 2 W/M.K." Https://My.Element14.Com/T-Global/Pc93-150x150x1-0/Thermal-Pad-1mm-2w-M-K-Grey/Dp/2466894 (Accessed.

[22] T. Global. "Pc94-150x150x1.0 -Thermal Pad, Non-Silicone, 150mm X 150mm X 1mm, 4 W/M.K." Https://My.Element14.Com/T-Global/Pc94-150x150x1-0/Thermal-Pad-1mm-4w-M-K-Red/Dp/2466897 (Accessed.

[23] J. Taylor, *Introduction To Error Analysis, The Study Of Uncertainties In Physical Measurements*. 1997.

Proceedings DOI: 10.21467/proceedings.141
ISBN: 978-81-957605-4-1

Series: AIJR Proceedings
ISSN: 2582-3922